Supplementary Information

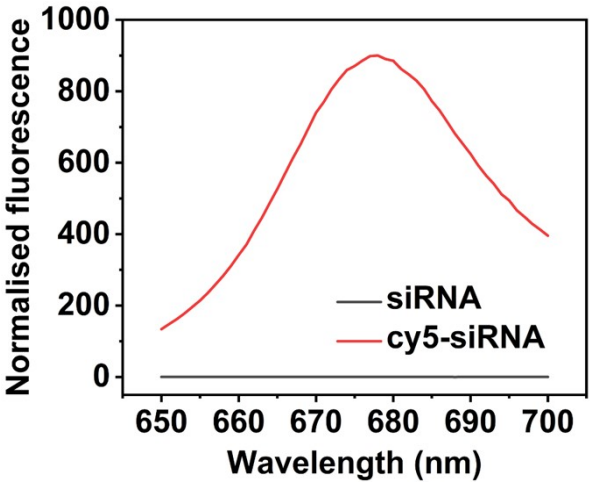

Figure S1. Fluorescence spectrophotometer analysis of siRNA and cy5-siRNA.

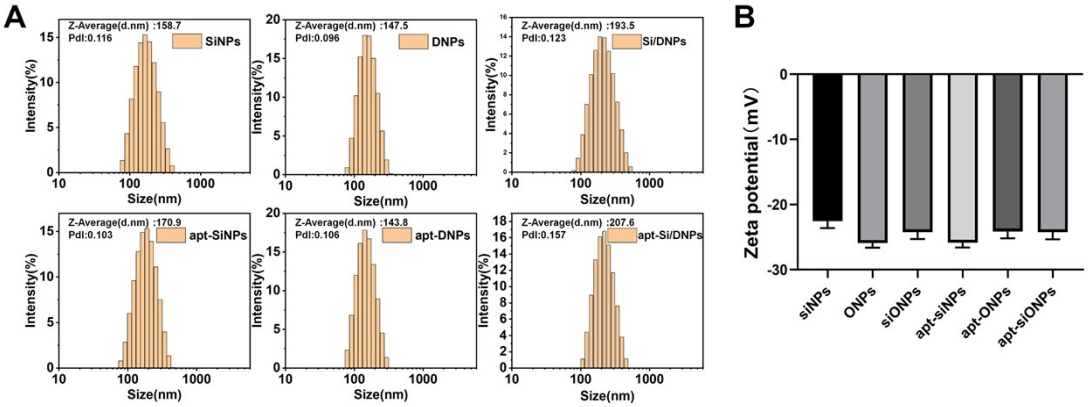

Figure S2. (A) Size and (B) Zeta potential of different samples measured by DLS.

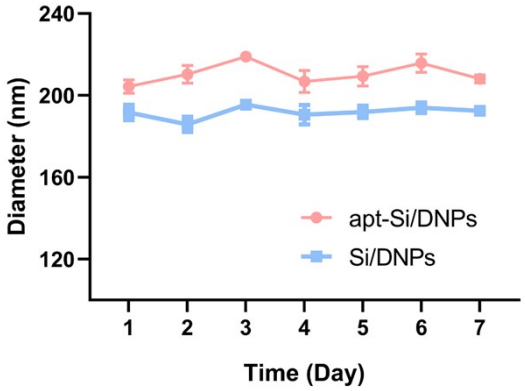

Figure S3. Time-dependent size stability of Si/DNPs and apt-Si/DNPs in PBS at 4°C. Data are shown as mean ± SD (n=3).

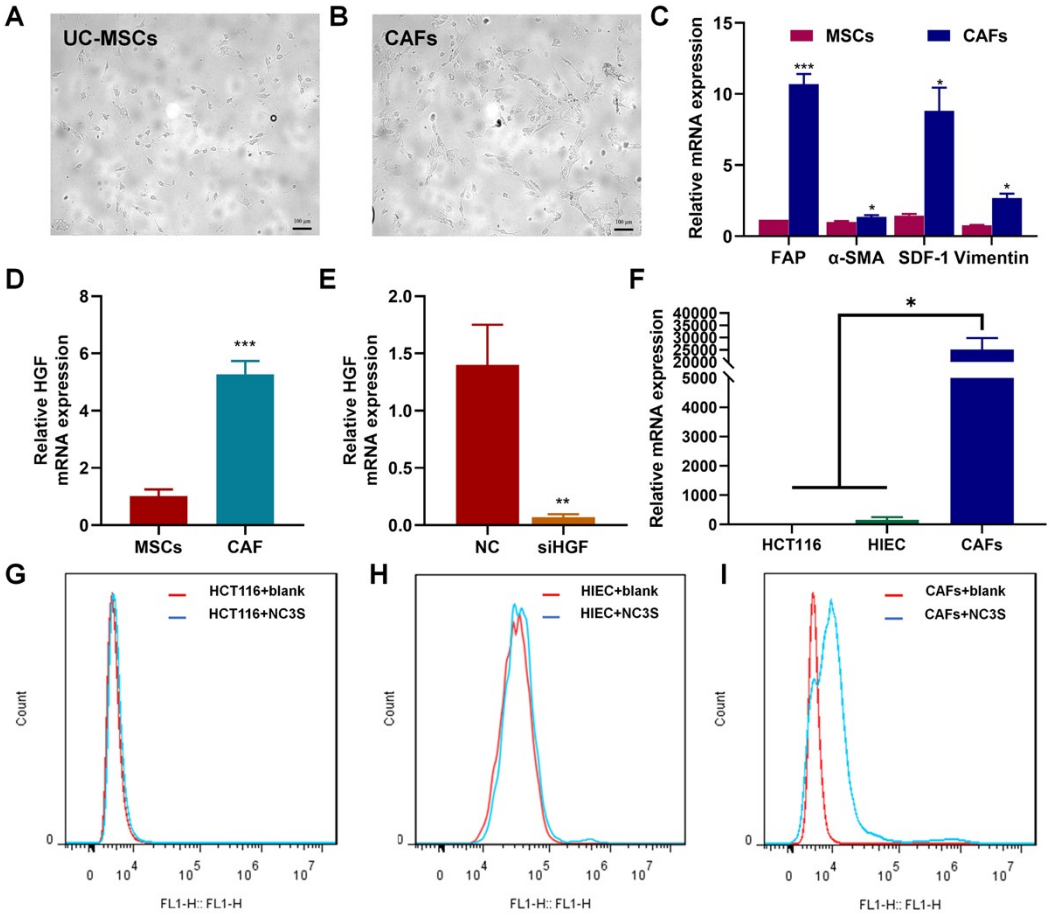

Figure S4. Characterization of CAFs. Morphology of (A) UC-MSCs and (B) CAFs. (C) The mRNA level of FAP, α-SMA, SDF-1 and vimentin was detected by rt-PCR, GAPDH was used as internal control. (D) The mRNA level of HGF in CAFs cells. (E) The mRNA level of HGF in CAFs cells transfected with siRNA target HGF. (F) Relative N-cadherin mRNA expression in HCT116, HIEC and CAFs cells was detected by real-time PCR. Flow cytometry assays for the conjunction of NC3S aptamer with (G) HCT116, (H) HIEC and (I) CAFs cells. *P < 0.05, **P < 0.01, ***P < 0.005.

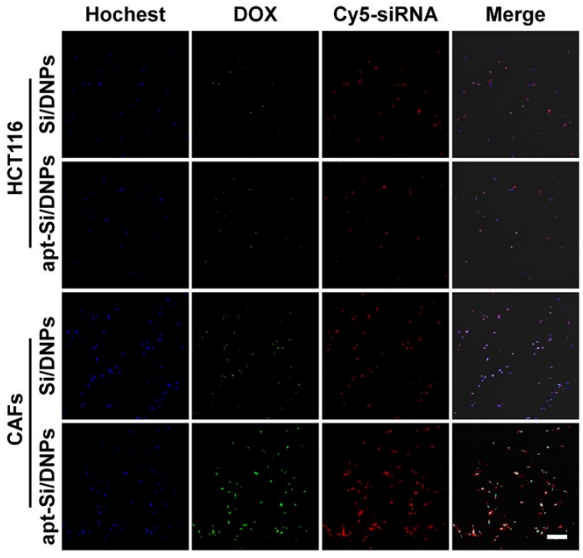

Figure S5. Cellular uptake assay of Si/DNPs and apt-Si/DNPs in CAFs and HCT116 cells. CLSM

images of CAFs and HCT116 cells after incubation with Si/DNPs and apt-Si/DNPs for 1 h. DOX (green) and siRNA labeled by Cy5 (red) were co-loaded into the nanoparticles. Scale bar, 200 μm.

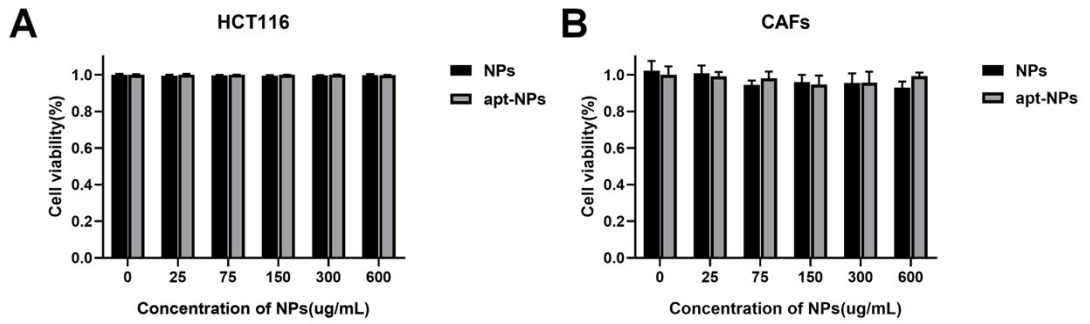

Figure S6. Cytotoxicity of free NPs and free apt-NPs against (A) HCT116 and (B) CAFs cells after 72 h incubation at different concentrations.

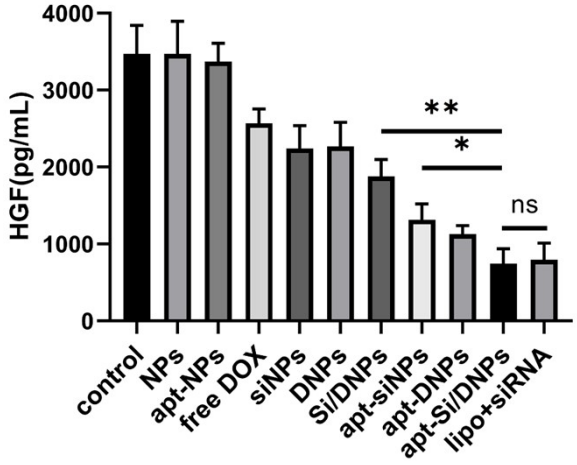

Figure S7. Quantitative analysis of HGF expression level through enzyme-linked immunosorbent assay (ELISA). *P < 0.05, **P < 0.01, NS no significance.

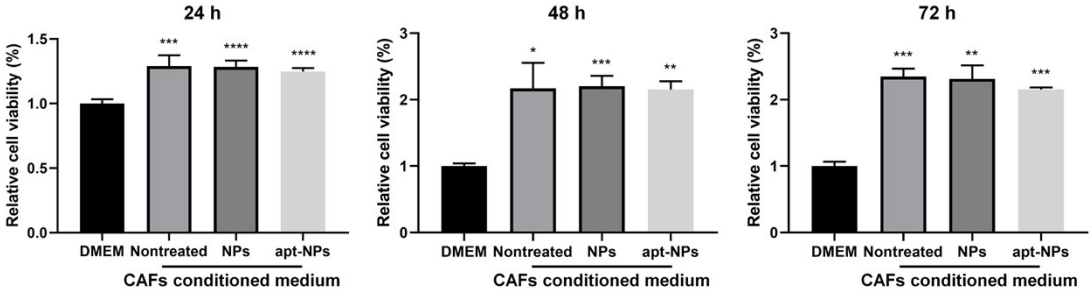

Figure S8. HCT 116 cell viability after incubated with the CAFs-conditioned medium (collected after treating with or without NPs and apt-NPs) for 24, 48 and 72 h. *P < 0.05, **P < 0.01, ***P < 0.005.

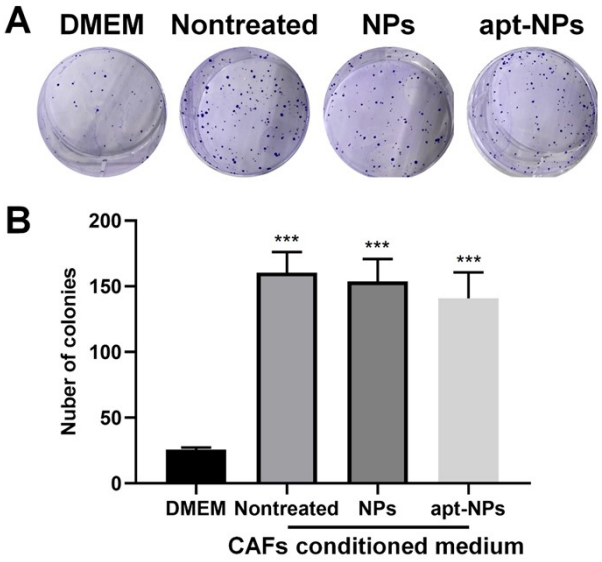

Figure S9. (A) HCT 116 cell clone formation after incubated with the CAFs-conditioned medium (collected after treating with or without NPs and apt-NPs) on day 14. (B) Quantitative analysis of the colony numbers of HCT116 cells. The values are the mean ± SD from three independent experiments. ***P<0.005.

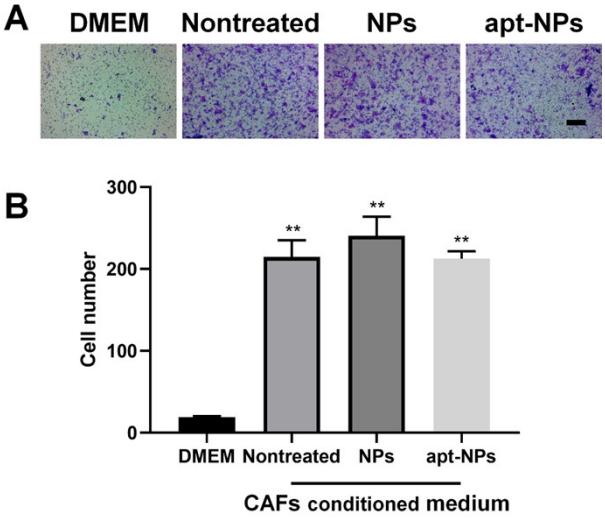

Figure S10. Images (A) and quantification analysis (B) of migrated HCT116 cells after incubated with CAF-CM collected after treating with or without NPs and apt-NPs. Scale bar, 200 μm. Data was exhibited as the mean ± SD (n = 4). **P < 0.01.

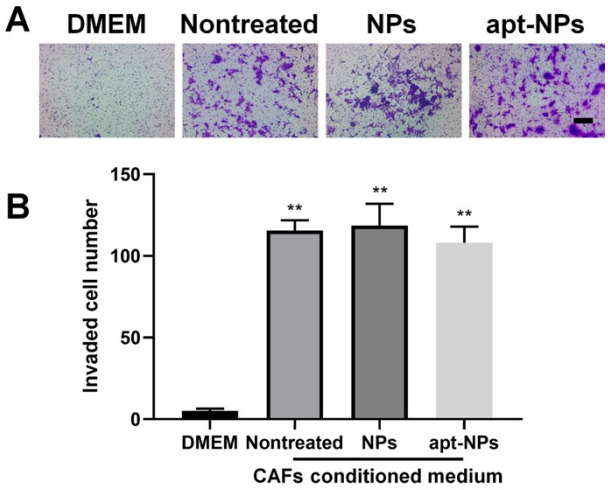

Figure S11. Images (A) and quantification analysis (B) of invaded HCT116 cells after incubated with CAF-CM collected after treating with or without NPs and apt-NPs. Scale bar, 200 μm. Data are shown as the mean ± SD (n = 4); **P<0.01.

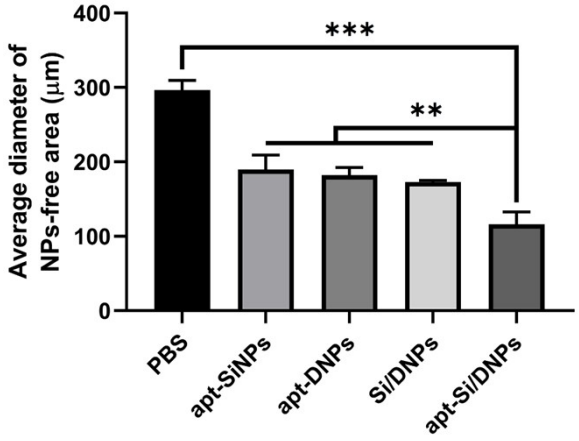

Figure S12. Quantification analysis of average diameter in nanoparticles-free region in 3D tumor spheres. **P<0.01, ***P<0.005.

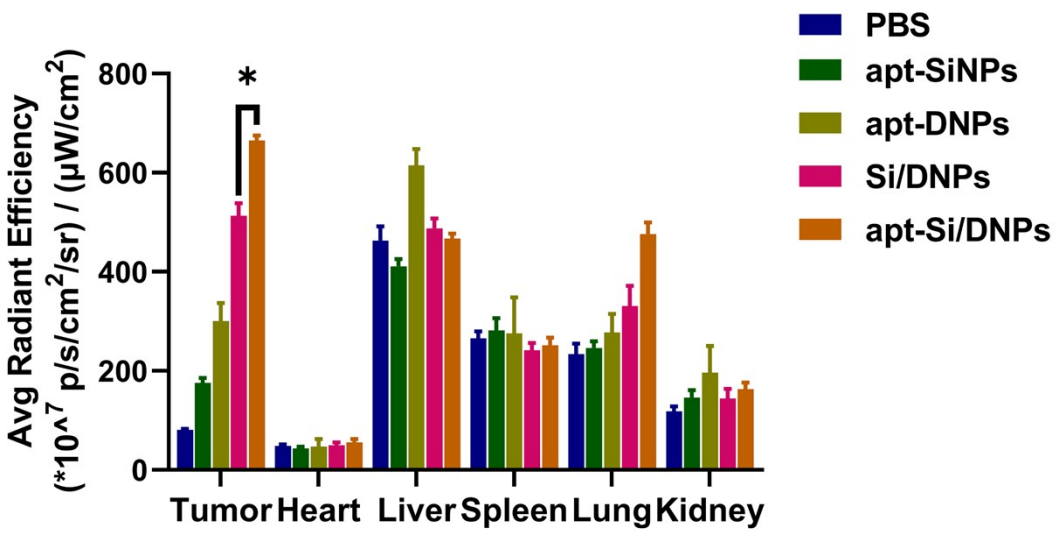

Figure S13. The corresponding average radiation efficiency of DiR@NPs in excised tumors and major organs at 48 h after test particle injection. *P < 0.05.

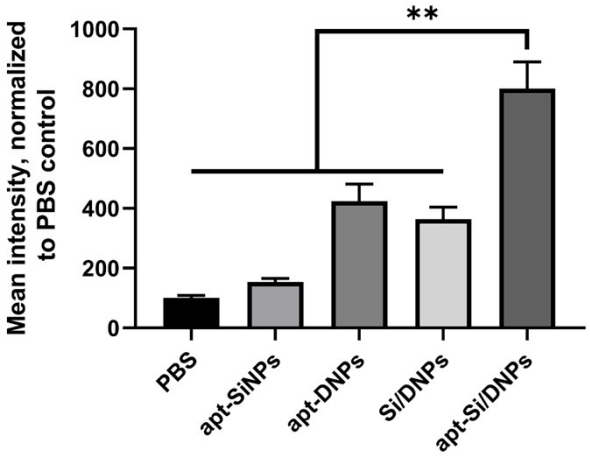

Figure S14. Quantitative results of CLSM images. Five randomly selected fields of each group were used for statistical analysis. **P < 0.01.

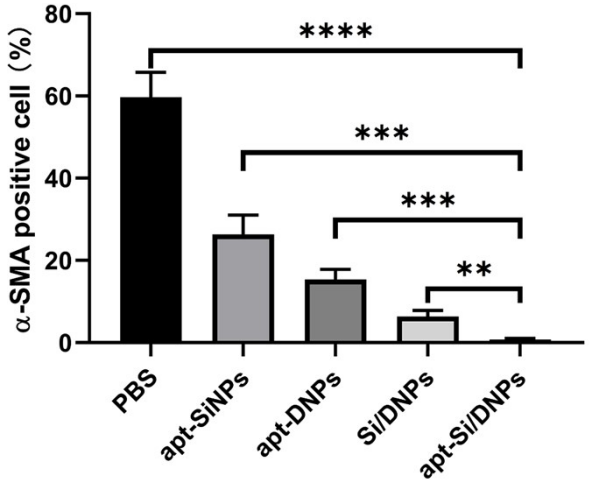

Figure S15. Quantitative analysis of α-SMA$^+$ cells of tumor sections in various formulation groups. **P < 0.01, ***P < 0.005.

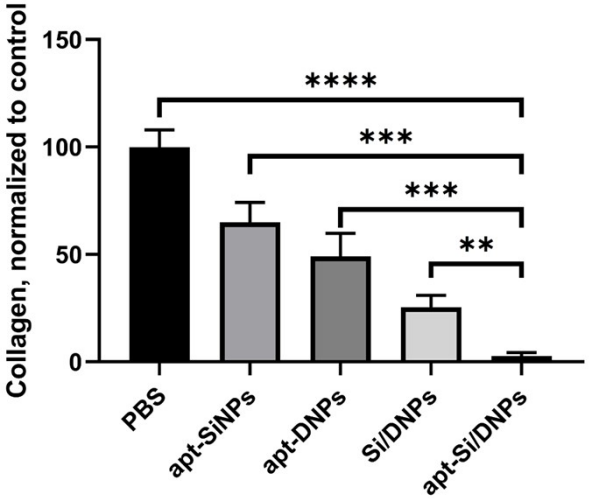

Figure S16. Quantitative analysis of collagen content in in various formulation groups by Image J. **P < 0.01, ***P < 0.005, ****P < 0.001.

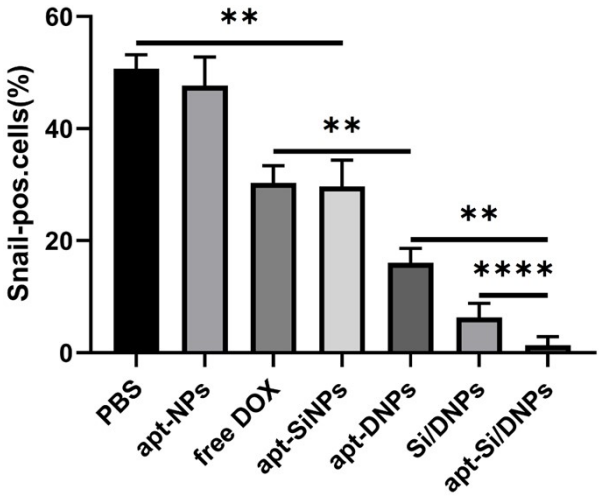

Figure S17. Corresponding quantification of Snail-positive cells of tumor sections in various formulation groups. **P < 0.01, ****P < 0.001.

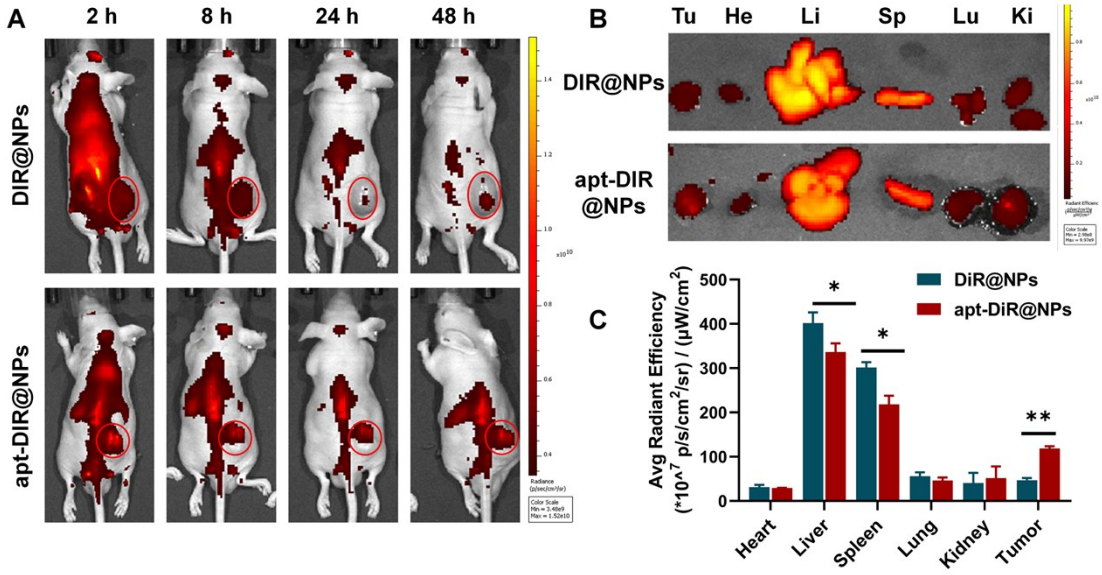

Figure S18. Biodistribution of NPs and apt-NPs. (A) Living body images of tumor-bearing mice at fixed timepoint. The tumor area is marked in red circles. (B) Representative images of excised tumors and major organs ex vivo. Tumor (Tu), heart (H), liver (Li), spleen (Sp), lung (Lu), and kidney (Ki). (C) The corresponding average radiation efficiency in excised tumors and important organs. *P < 0.05, **P < 0.01.

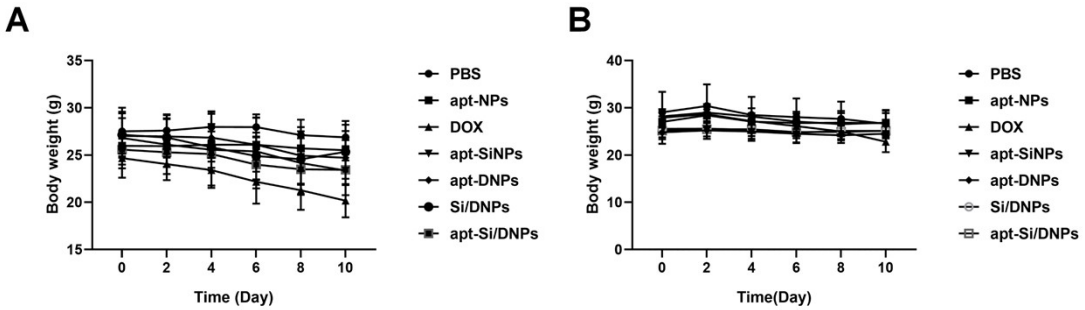

Figure S19. Influences of various nanoemulsions on body weight of HCT116 (A) subcutaneous xenograft mice and (B) pulmonary metastasis mice.

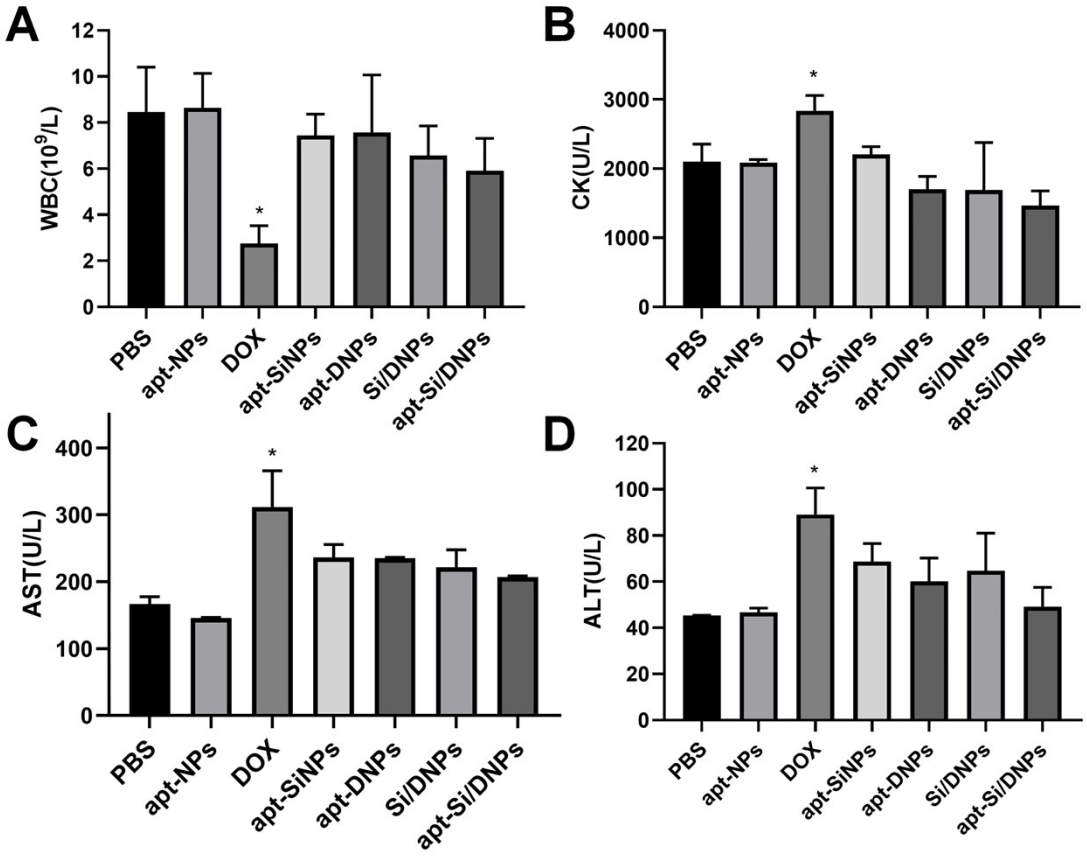

Figure S20. Experiment results of (A) white blood cells count in whole blood, (B) CK, (C) ALT, and (D) AST in plasma samples from subcutaneous xenograft mice. *P < 0.05.

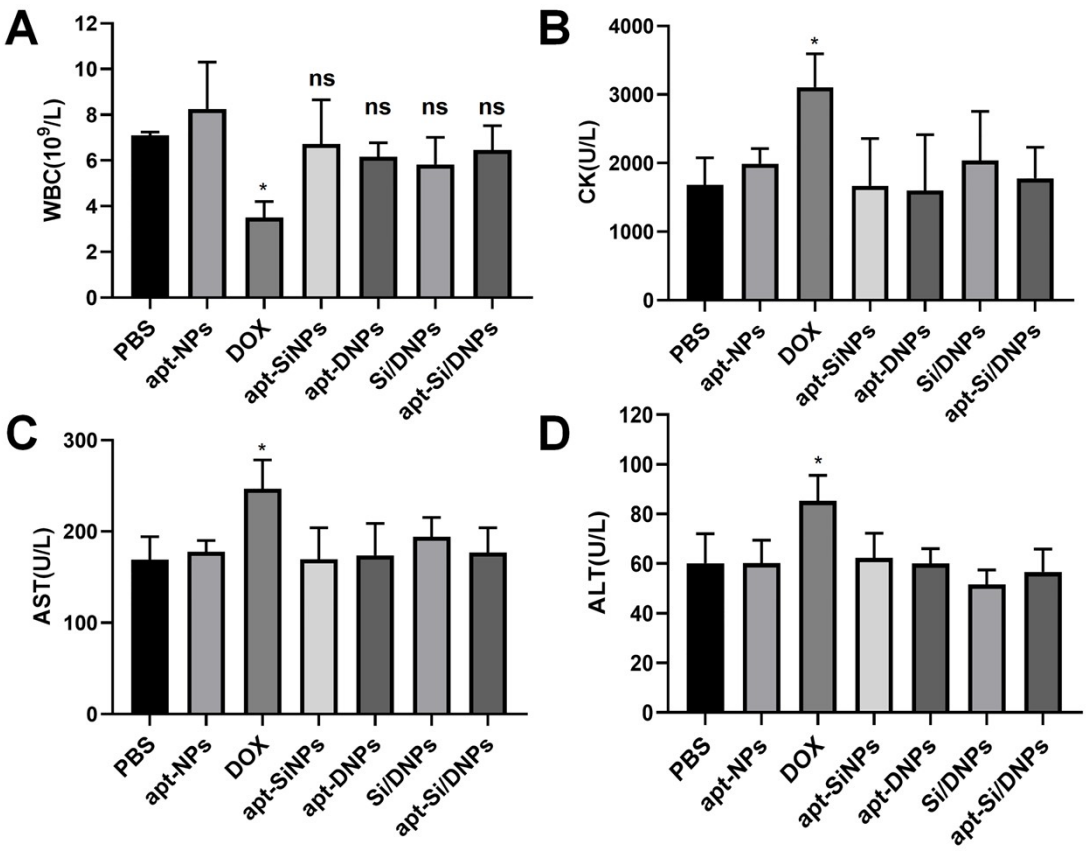

Figure S21. Experiment results of (A) white blood cells count in whole blood, (B) CK, (C) ALT, and (D) AST in plasma samples from pulmonary metastasis mice. *P < 0.05.

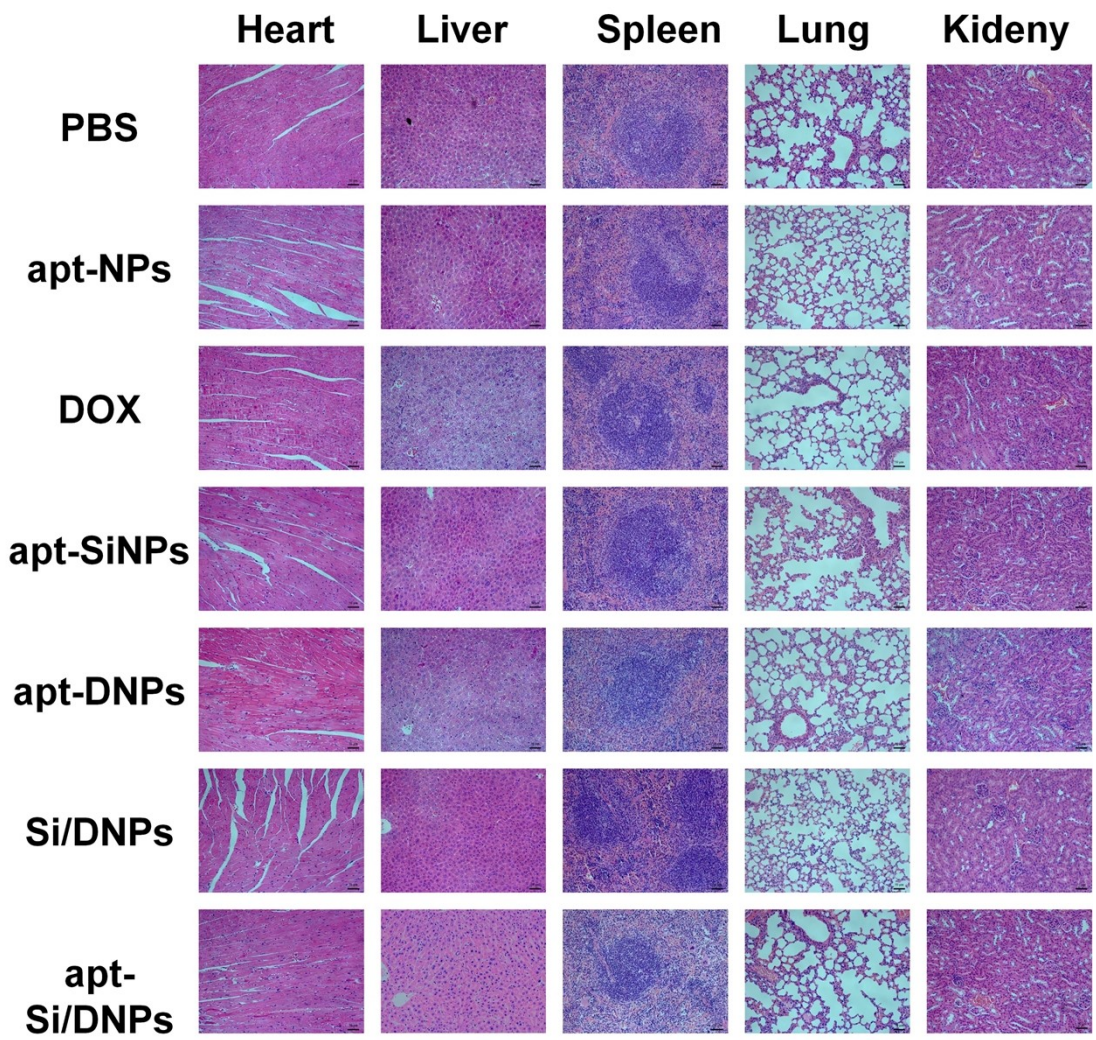

Figure S22. Representative images of major organs obtained from subcutaneous xenograft mice receiving various treatment in H&E staining histological. Scale bar, 50 μm

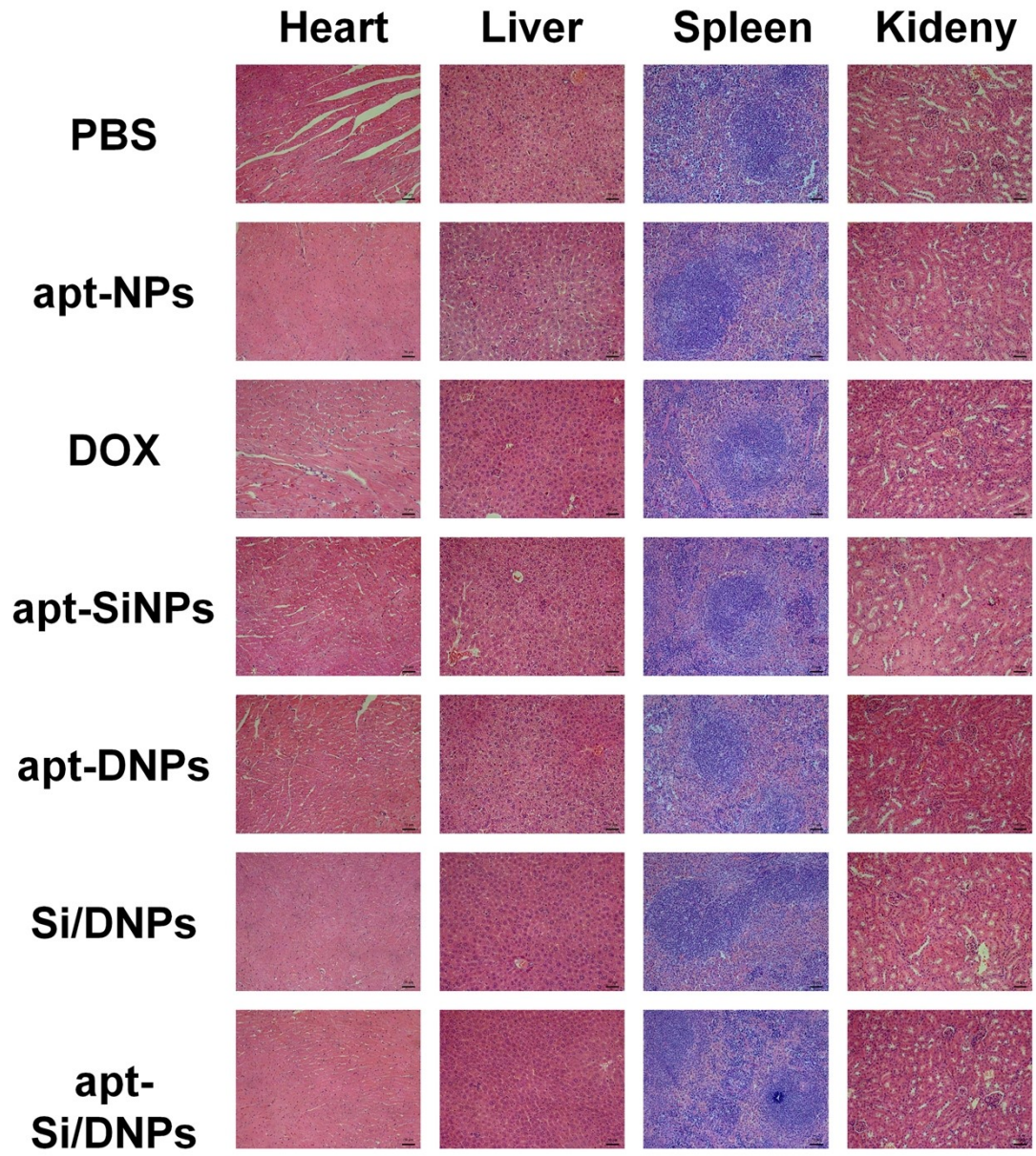

Figure S23. Representative images of major organs obtained from pulmonary metastasis mice receiving various treatment in H&E staining histological. Scale bar, 50 μm.

Table 1. Encapsulation efficiency (EE%) and drug loading (DL%) content of different nanoparticle nanoemulsions.

Samples	EE of siRNA-HGF (%)	EE of DOX (%)	DL of siRNA-HGF (%)	DL of DOX (%)
SiNPs	**84.6±3.5**	-	**0.5± 0.038**	-
DNPs	-	**55.6± 3.4**	-	**1.6±0.3**
Si/DNPs	**92.4±1.8**	**62.4±8.1**	**0.5±0.075**	**2.1±0.7**

Table 2. Sequences of siRNA used in RNA interference assay

Name	sequences
Negative control (siNC)	sense strand:5′-UUCUCCGAACGUGUCACGUTT-3′ antisense strand: 5′-ACGUGACACGUUCGGAGAATT-3′
Hepatocyte growth factor (siHGF)	sense strand:5′-CCAUGAAUUUGACCUCUAUTT-3′ antisense strand: 5′-AUAGAGGUCAAAUUCAUGGTT-3′

Table 3. Primer sequences used in real-time PCR

Name	Sequences
GAPDH	Forward: 5′-GAGAGACCCTCACTGCTG-3′ Reverse: 5′-GATGGTACATGACAAGGTGC-3′
Vimentin	Forward: 5′-AGTCCACTGAGTACCGGAGAC-3′ Reverse: 5′-CATTTCACGCATCTGGCGTTC-3′
FAP	Forward: 5′-ATGAGCTTCCTCGTCCAATTCA-3′ Reverse: 5′-AGACCACCAGAGAGCATATTTTG-3′
SDF-1	Forward: 5'-GTTTGTGCTGTGGTGTGTCC-3' Reverse: 5'-ATACTAAGGTTGGGGGAGGTG-3'
α-SMA	Forward: 5′-AAAAGACAGCTACGTGGGTGA-3′ Reverse: 5′-GCCATGTTCTATCGGGTACTTC-3′